Absolute Navigation Performance of the Orion Exploration Flight Test 1

Renato Zanetti[1], Greg Holt[2], Robert Gay[3], and Christopher D'Souza[4]
NASA Johnson Space Center, Houston, Texas 77058.

Jastesh Sud[5], Harvey Mamich[6], and Michael Begley[7]
Lockheed Martin Space Systems Company, Denver, CO 80201

Ellis King[8] and Fred D. Clark[9]
Draper Laboratory, Houston, Texas 77058

Launched in December 2014 atop a Delta IV Heavy from the Kennedy Space Center, the Orion vehicle's Exploration Flight Test-1 (EFT-1) successfully completed the objective to stress the system by placing the un-crewed vehicle on a high-energy parabolic trajectory replicating conditions similar to those that would be experienced when returning from an asteroid or a lunar mission. Unique challenges associated with designing the navigation system for EFT-1 are presented with an emphasis on how redundancy and robustness influenced the architecture. Two Inertial Measurement Units (IMUs), one GPS receiver and three barometric altimeters (BALTs) comprise the navigation sensor suite. The sensor data is multiplexed using conventional integration techniques and the state estimate is refined by the GPS pseudorange and deltarange measurements in an Extended Kalman Filter (EKF) that employs UDU factorization. The performance of the navigation system during flight is presented to substantiate the design.

---

[1] GN&C Autonomous Flight Systems Engineer, Aeroscience and Flight Mechanics Division, EG6, 2101 NASA Parkway
[2] Deputy Orion Navigation Lead, Flight Operations Directorate, CM55, 2101 NASA Parkway.
[3] Orion Navigation Lead, Aeroscience and Flight Mechanics Division, EG6, 2101 NASA Parkway.
[4] Navigation Technical Discipline Lead, Aeroscience and Flight Mechanics Division, EG6, 2101 NASA Parkway.
[5] Software Engineer Staff, M/S B3003, P.O. Box 179
[6] Orion Navigation Lead, M/S B3003, P.O. Box 179
[7] Orion GN&C Subsystem Deputy and CPE, M/S B3003, P.O. Box 179
[8] Senior Member, Technical Staff, 17629 El Camino Real, Suite 470
[9] Principal Member, Technical Staff, 17629 El Camino Real, Suite 470

Nomenclature

b, $\mathbf{b}$	Bias states
$\mathbf{e}$	Estimation error
$\mathbf{f}$	Nonlinear state dynamics function
$\mathbf{F}$	Jacobian of state dynamics
$\mathbf{g}$	Gravity vector
$\mathbf{G}$	Gravity gradiant
$\mathbf{h}$	Nonlinear measurement function
$\mathbf{H}$, or $\widetilde{\mathbf{H}}$	Measurement mapping matrix
$\mathbf{I}$	Identity matrix
$\mathbf{K}$	Kalman gain matrix
$\mathbf{p}$	parameters state vector
$\mathbf{P}$	Estimation error covariance
$\mathbf{q}_{a\to b}$	(Right) quaternion expressing the rotation from frame "a" to frame "b"
$\mathbf{Q}$	Process noise power spectral density
$\overline{\mathbf{Q}}$	Process noise covariance
$\mathbf{r}$	Position vector
$\mathbf{R}$	Measurement error covariance
$\mathbf{s}$	scale factor vector
$\mathbf{S}$	scale factor matrix
t	time
$\mathbf{T}_a^b$	Direction cosine matrix from frame "a" to frame "b"
$\mathbf{U}$	Element of $\mathbf{UDU}^{\mathrm{T}}$ covariance factorization
$\mathbf{v}$	Velocity vector
$\mathbf{x}$ or $\mathbf{X}$	State vector
$\mathbf{y}$ or $\tilde{\mathbf{y}}$	Measurement vector

$\boldsymbol{\gamma}$	Gyro non-orthogonality vector
$\boldsymbol{\Gamma}$	Gyro non-orthogonality matrix
δ	deviation or error, e.g. $\delta\mathbf{x}$
Δ	variation or error
ϵ, $\boldsymbol{\epsilon}$	Measurement residual
η, $\boldsymbol{\eta}$	Measurement noise
$\boldsymbol{\theta}$	Attitude Rotation Vector
$\boldsymbol{\phi}$	attitude error state
$\boldsymbol{\Phi}$	State transition matrix
$\boldsymbol{\nu}$	Process noise
$\boldsymbol{\omega}$	Angular velocity
$\boldsymbol{\xi}$	Accelerometer misalignment/non-orthogonality vector
$\boldsymbol{\Xi}$	Accelerometer misalignment/non-orthogonality matrix
σ	Standard deviation

Diacritic

$\hat{\mathbf{x}}$	Estimated "$\mathbf{x}$"

Subscript and Superscript

a	accelerometer
b	Orion body coordinates
c	IMU-Fixed case coordinates
g	gyro
i	Inertial coordinates (ICRF a.k.a. ECI)
$-$	value prior to the measurement update
$+$	value posterior to the measurement update

I. Introduction

The Orion vehicle, designed to take men back to the Moon and beyond, successfully completed its first flight test, EFT-1 (Exploration Flight Test-1), on December 5th, 2014. The main objective of the test was to demonstrate the capability to re-enter into the Earth's atmosphere and safely splash-down into the Pacific Ocean. This un-crewed mission completed two orbits around Earth, the second of which was highly elliptical with an apogee altitude of approximately 5908 km, higher than any vehicle designed for humans has been since the Apollo program. The trajectory was designed in order to test a high-energy re-entry similar to those crews will undergo during lunar missions. The mission overview is shown in Figure 1.

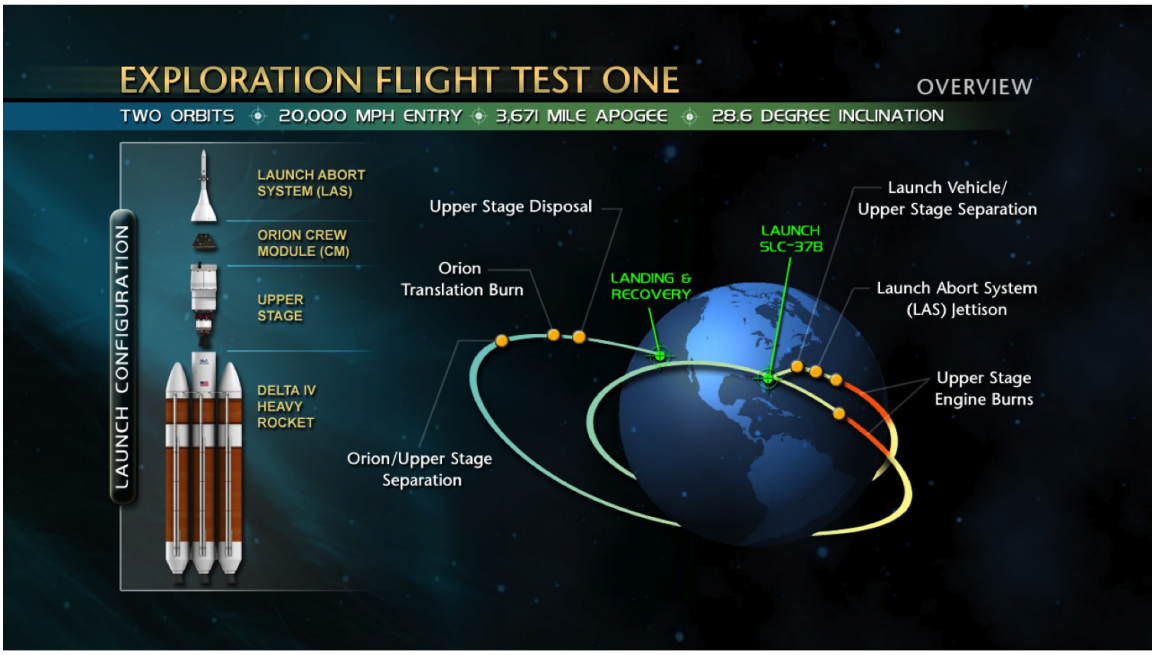

Fig. 1 EFT-1 Mission Profile

The first of the two orbits starts with the conclusion of the first upper stage burn (SECO1); towards the end of the first orbit, the upper stage ignites again to raise the apogee, the conclusion of this second upper stage burn (SECO2) places Orion on its final highly elliptical orbit. Following apogee the Orion capsule separates from the upper stage, from this moment on Orion is responsible for its own onboard Guidance, Navigation, and Control (GN&C) to safely take the vehicle to splash-down in the Pacific Ocean; although the absolute navigation system was active during the entire flight.

The objective of this paper is to document the performance of the absolute navigation system during EFT-1, which relies on the classic extended Kalman filter (EKF) [1]. A prior version of this work introduced the navigation design [2], while pre-flight simulation performance was shown in Ref. [3]. The UDU factorization as introduced by Bierman is employed in the filter design [4], and measurements are included as scalars employing the Carlson [5] and Agee-Turner [6] Rank-One updates. The possibility of considering only some of the filter's states (rather than estimating all of them [7]) is included in the design [8], and a method to eliminate low-elevation satellites is used that does not rely on a fixed masking angle.

This paper focuses on the performance of the EFT-1 absolute navigation system after lift-off and while incorporating GPS measurements. One of the EFT-1 mission goals was to test the new GPS receiver's clock stability, clock filter state restarts, and high altitude GPS processing.

This paper is organized as follows. First, the overall absolute navigation architecture is introduced, followed by the design of the 40 Hz propagator and the 1 Hz EKF. The introduction of the design is followed by the presentation of the actual flight data, and finally some conclusions are drawn.

II. Absolute Navigation Architecture

Two Orion Inertial Measurement Units (OIMUs), a GPS receiver (GPSR) and three barometric altimeters (BALTs) comprise the Orion sensor suite. The OIMUs provide integrated accelerometer and gyro data at high rate. The inertial state is propagated at 40 Hz and is updated by GPSR pseudorange (PR) and deltarange (DR) measurements at 1 Hz. The attitude of the vehicle is initialized by gyro-compassing, is updated with integrated velocity (IV) measurements while on the pad, and is updated with GPSR measurements, when available during flight.

The BALTs measurements are not incorporated into the navigation filter, but they are used as backups by the Navigation Fault Detection, Isolation, and Recovery algorithm (FDIR). In the event the GPSR fails or if the filtered solution has diverged, the FDIR logic autonomously selects the BALT output as the primary source of altitude. The logic accomplishes this by comparing the EKF covariance in the radial direction with a parameterized threshold value. FDIR also checks the

filter's performance by monitoring the measurements' acceptances and rejections.

Each of the flight computers contains two instances of the navigation filter, each slaved to a different OIMU. The purpose of this design is to allow for an instantaneous recovery after an OIMU failure without having to go to a transient period to estimate the OIMU error states or for the filter to re-converge. Each OIMU is tied to a navigation channel, each channel contains several Computer Software Units (CSUs): an IMU Subsystem Operating Program (IMUSOP) that is responsible for parsing the OIMU data, a Coarse Align (CAlign) CSU that is responsible for providing a crude estimate of the initial attitude on the pad, a Filtered Navigator (FiltNav) CSU that is responsible for multiplexing the OIMU data with the GPS updates and an Inertial Navigator (INRTLNAV) CSU that is responsible for maintaining an unaided (OIMU-only) state. INRTLNAV and FiltNav have counterparts on the 1 Hz side. The Inertial Navigator Gravity (InrtlNavGrav) and Extended Kalman Filter (EKF) CSUs on the 1 Hz side provide a higher-order gravity estimate to INRTLNAV and state updates to FiltNav, respectively.

IMU FDIR and GPS FDIR live outside of the channels and are responsable for detecting faulty sensor data. The outputs of the two channels are received by Navigation FDIR (NAVFDIR) CSU which selects the primary state. The NAVFDIR scheme relies on the IMUFDIR outputs and performs additional tests on the filtered solution. One of the checks it relies on is the percentage of PR/DR measurements being accepted by each channel.

Prior to launch the filter is initialized with the Coarse Align attitude and an inertial position derived from the current time and the coordinates of the pad. This pre-launch navigation phase is called Fine Align and the only measurement active in this mode is Integrated Velocity (IV), which is a pseudo-measurement consisting of a zero change of Earth-referenced position over a 1 second interval. GPSR measurements are not available during fine align. The main purpose of fine align is to better estimate the attitude.

The ascent phase is divided in two parts, the first when GPSR measurements are not enabled (Ascent Without GPS), and the second when they are (Ascent With GPS). The only difference between Fine Align and Ascent Without GPS is that the IV measurement processing is inhibited in the latter. The maximum number of processable GPS measurements is set to 12, which is a large

enough number to obtain good performance while keeping the throughput reasonably low. To avoid possible transient issues the very first PR measurement is not processed. Counters of consecutive GPS measurements are kept and the measurements are included in the solution only when the corresponding counter value is greater than one. After a long blackout the covariance becomes very large and the inclusion of nonlinear measurements creates problems. In particular, inclusion of the DR measurement creates convergence issues. Through numerical simulation it was determined that allowing for multiple PRs ($\sim$30) to be processed before incorporating a DR mitigates this issue because the PRs shrink the uncertainty before DRs are introduced. If a satellite is not present for a single cycle, the corresponding counter is not reset and if the satellite comes back it is immediately used as a measurement. If the satellite is absent for more than a cycle the corresponding counter is reset.

The GPSR provides an estimate of the PR variance together with the measurement. The EKF uses this variance estimate together with a PR variance floor parameter which limits the minimum value of PR measurement variance used in incorporating the measurement into the filter. Underweighting is applied when the estimated measurement has an uncertainty greater than 100 ft.

GPSR measurements are processed throughout the orbit phase and during entry when available. A GPS blackout was expected and experienced during entry. In order to process latent GPS measurements the EKF necessitates to back-propagate its current state estimate to the measurement time. This task is made possible by a 4Hz buffer of OIMU data provided to EKF by FiltNav. When accelerating fast under the chutes during entry, the attitude dynamics are not accurately represented by the 4Hz IMU buffer. Therefore PR and DR measurements are inhibited above a certain angular velocity.

A major frame is a 1 Hz cycle and is denoted by a capital letter (A, B, C, etc.) individual EKF calls are denoted by their major frame. A minor frame is a 40 Hz cycle and is denoted by a number from 0 to 39, individual FiltNav calls are denoted by both their major and minor frame (A0, A1, A39, B0, etc.). FiltNav receives EKF data at minor frame 0, that is to say that FiltNav B0 receives EKF data A, C0 receives EKF data B, etc. The EKF receives FiltNav data from minor frame 0, that is to say that EKF A receives FiltNav A0 data, B receives FiltNav B0 data, etc. As a consequence,

the data provided by the EKF at any major frame (e.g. C) is time-tagged with the same time as the output of the first FiltNav call of this same major cycle (e.g. C0). Another consequence is that FiltNav receives an EKF update that is exactly one major frame old, e.g. FiltNav B0 receives an EKF update from major frame A that is time-tagged with the same time as FiltNav A0. The data transfer is shown in Figure 2.

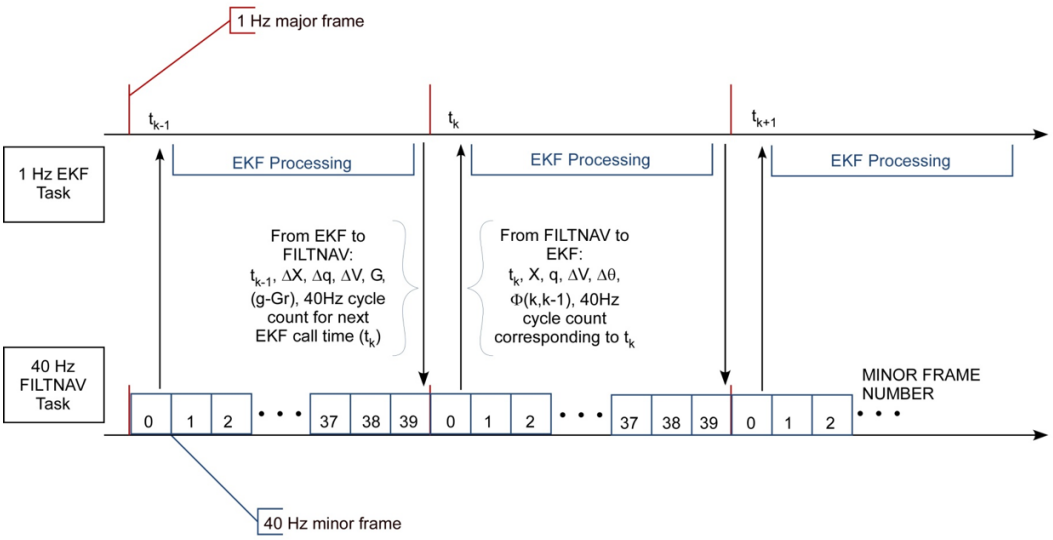

Fig. 2 Data Transfer Between EKF and FiltNav

III. Filtered Navigator Design

The Filtered Navigator is a flight software CSU running at 40 Hz responsible for providing users with high rate inertial position, velocity, and attitude. The 1 Hz EKF also utilizes the propagated position, velocity, and attitude from FiltNav, but also need the IMU's accumulated $\Delta\mathbf{v}$ and $\Delta\boldsymbol{\theta}$ measurements (both compensated and non-compensated) in order to compute the dynamics partials and the state transition matrix, which is needed by the EKF to propagate forward in time the estimation error covariance matrix.

A. IMU Measurements Accumulation

Accumulated IMU measurements and the attitude quaternion are buffered by FiltNav at 4 Hz in order to back propagate the EKF state and process latent measurements.

FiltNav receives from the IMU SOP four to six new samples (nominally five) of 200 Hz incremental gyro and accelerometer measurements: $\Delta\boldsymbol{\theta}^b_{k,j}$ and $\Delta\mathbf{v}^b_{k,j}$. The subscript k indicates the 40 Hz FiltNav cycle, the subscript j ranging from one to six indicates the 200 Hz sample, and the superscript b indicates the Orion body frame. The IMU case frame c is defined such that the x-axis of the gyro is the reference direction with the xy-plane being the reference plane; the y- and z-axes are not mounted perfectly orthogonal to it (this is the reason of the absence of a full misalignment/nonorthogonality matrix as there is in the accelerometer model).

The gyro measurement in the IMU case frame is given by

$$\Delta\boldsymbol{\theta}^c_{k,j} = \mathbf{T}^c_b\,\Delta\boldsymbol{\theta}^b_{k,j} \tag{1}$$

where $\mathbf{T}^c_b$ is the matrix that transforms Orion body coordinates into IMU case coordiantes. The compensated gyro measurement is obtained using the 1 Hz estimates of the gyro bias $\hat{\mathbf{b}}_g$, scale factor errors $\hat{\mathbf{s}}_g$, and non-orthogonality $\hat{\boldsymbol{\gamma}}_g$, all three of these vectors are coordinatized in the IMU case frame. Define matrix $\boldsymbol{\Gamma}_g$, as

$$\hat{\boldsymbol{\Gamma}}_g = \begin{bmatrix} 0 & 0 & 0 \\ \hat{\gamma}_z & 0 & 0 \\ \hat{\gamma}_y & \hat{\gamma}_x & 0 \end{bmatrix}$$

and $\mathbf{S}_g$ as

$$\hat{\mathbf{S}}_g = \begin{bmatrix} \hat{s}^g_x & 0 & 0 \\ 0 & \hat{s}^g_y & 0 \\ 0 & 0 & \hat{s}^g_z \end{bmatrix}$$

The compensated gyro measurement $\Delta\hat{\boldsymbol{\theta}}^c_{k,j}$ is

$$\Delta\hat{\boldsymbol{\theta}}^c_{k,j} = \left(\mathbf{I}_3 - \hat{\boldsymbol{\Gamma}}_g - \hat{\mathbf{S}}_g\right)\Delta\boldsymbol{\theta}^c_{k,j} - \hat{\mathbf{b}}_g \tag{2}$$

where $\mathbf{I}_3$ is the 3×3 identity matrix. The accumulated raw and compensated gyro measurements are initialized at zero and computed by FiltNav as

$$\Delta\boldsymbol{\theta}^{accum,c}_{k,j} = \Delta\boldsymbol{\theta}^{accum,c}_{k,j-1} + \Delta\boldsymbol{\theta}^c_{k,j} \tag{3}$$

$$\Delta\hat{\boldsymbol{\theta}}^{accum,c}_{k,j} = \Delta\hat{\boldsymbol{\theta}}^{accum,c}_{k,j-1} + \Delta\hat{\boldsymbol{\theta}}^c_{k,j} \tag{4}$$

with the understanding that the following two epochs are the same: $t_{k,0} = t_{k-1,N}$, where N is the last of the 200 Hz samples (either the fourth, fifth, or sixth). Notice that by adding quantities in different frames (the case frame rotates between one measurement to the next) an approximation is made. This approximation is deemed acceptable because these quantities are solely used in the calculation of partials of the dynamics and the covariance matrix, which is a linearized and approximated quantity in any case. This $\Delta\boldsymbol{\theta}$ buffers are not in the actual propagation of any state.

The raw accelerometer measurement is defined as the measurement in the IMU case frame

$$\Delta\mathbf{v}_{k,j}^{c} = \mathbf{T}_{b}^{c}\,\Delta\mathbf{v}_{k,j}^{b} \tag{5}$$

The compensated accelerometer measurement is obtained using the 1 Hz estimates of the accelerometer bias $\hat{\mathbf{b}}_a$, scale factors $\hat{\mathbf{s}}_a$, and non-orthogonality/misalignment $\hat{\boldsymbol{\xi}}_a$, all three these vectors are coordinatized in the IMU case frame. Define matrix $\hat{\boldsymbol{\Xi}}_a$, as

$$\hat{\boldsymbol{\Xi}}_a = \begin{bmatrix} 0 & \hat{\xi}_{xy} & \hat{\xi}_{xz} \\ \hat{\xi}_{yx} & 0 & \hat{\xi}_{yz} \\ \hat{\xi}_{zx} & \hat{\xi}_{zy} & 0 \end{bmatrix}$$

and $\mathbf{S}_a$ as

$$\hat{\mathbf{S}}_a = \begin{bmatrix} \hat{s}_x^a & 0 & 0 \\ 0 & \hat{s}_y^a & 0 \\ 0 & 0 & \hat{s}_z^a \end{bmatrix}$$

The compensated accelerometer measurement in the inertial frame $\Delta\hat{\mathbf{v}}_{k,j}^{i}$ is

$$\Delta\hat{\mathbf{v}}_{k,j}^{i} = \mathbf{T}_{c}^{i}\left[\left(\mathbf{I}_3 - \hat{\boldsymbol{\Xi}}_a - \hat{\mathbf{S}}_a\right)\Delta\mathbf{v}_{k,j}^{c} - \hat{\mathbf{b}}_a\right] \tag{6}$$

The accumulated raw and compensated accelerometer measurements are initialized at zero and computed by FiltNav as

$$\Delta\mathbf{v}_{k,j}^{accum,c} = \Delta\mathbf{v}_{k,j-1}^{accum,c} + \Delta\mathbf{v}_{k,j}^{c} \tag{7}$$

$$\Delta\hat{\mathbf{v}}_{k,j}^{accum,i} = \Delta\hat{\mathbf{v}}_{k,j-1}^{accum,i} + \Delta\hat{\mathbf{v}}_{k,j}^{i} \tag{8}$$

Only the accumulated raw measurement contains the approximation of adding quantities in slightly different frames (the case frame rotates between measurements), once again this approximation

is deemed acceptable because these quantities are solely used in the calculation of the covariance matrix. The compensated accumulated accelerometer measurement, on the other hand, is used to propagate the state; however no approximation is made since the accumulation occurs in the inertial frame.

In order to reduce computations, gravity is only evaluated once a second and the 40 Hz in-between values needed by FiltNav are calculated with a first order Taylor series truncation. FiltNav receives the gravity gradient $\mathbf{G}(\mathbf{r}^*)$ and the quantity $\mathbf{g}(\mathbf{r}^*) - \mathbf{G}(\mathbf{r}^*)\,\mathbf{r}^*$ from the EKF, where $\mathbf{g}$ is the gravity vector and $\mathbf{r}^*$ is the vehicle's inertial position and the center of the Taylor series. These two quantities are used rather than $\mathbf{g}(\mathbf{r}^*)$, $\mathbf{G}(\mathbf{r}^*)$, and $\mathbf{r}^*$ because it reduces overall computations ($\mathbf{g}(\mathbf{r}^*) - \mathbf{G}(\mathbf{r}^*)\,\mathbf{r}^*$ is calculated only once per second instead of once per 40 Hz call) and because it reduces the amount of data exchanged between rate groups ($\mathbf{r}^*$ is not passed from the EKF to FiltNav, only the delta state update is). All these quantities are calculated at the EKF calling time, hence they are nominally one second old when received by FiltNav and they are used to propagate position and velocity until they are almost two seconds old. The gravity at any location $\mathbf{r}$ is obtained truncating after the first-order in $\mathbf{r}$ as

$$\mathbf{g}(\mathbf{r}) \;\approx\; \mathbf{g}(\mathbf{r}^*) + \mathbf{G}(\mathbf{r}^*)\,[\mathbf{r} - \mathbf{r}^*] = \mathbf{G}(\mathbf{r}^*)\mathbf{r} + [\mathbf{g}(\mathbf{r}^*) - \mathbf{G}(\mathbf{r}^*)\mathbf{r}^*] \tag{9}$$

This is the equation associated with the propagation of the state (position and velocity) and the covariance (of the position and velocity). This above approximation is found to be more than sufficient and the higher-order terms in the Taylor series are found to be smaller than the errors due to the truncation of the gravity field.

Define t_0 as the beginning of the time propagation step, and $\mathbf{a}_1$ as

$$\mathbf{a}_1(t_0) = \mathbf{G}(\mathbf{r}^*)\mathbf{r}_0 + \{\mathbf{g}(\mathbf{r}^*) - \mathbf{G}(\mathbf{r}^*)\mathbf{r}^* + \mathbf{a}_s(t_0)\} \tag{10}$$

where $\mathbf{a}_s(t_0)$ is the compensated sensed acceleration from the IMU, i.e. the accelerometer sculled measurement compensated with the known EKF estimates of the IMU errors and coordinatized in the inertial frame. Define $\mathbf{a}_2$ as

$$\mathbf{a}_2 \;=\; \mathbf{G}(\mathbf{r}_0)\mathbf{v}_0 \tag{11}$$

FiltNav propagates position and velocity at 200 Hz using the following equations at each step

$$\mathbf{v} \approx \dot{\mathbf{r}}_0 + \mathbf{a}_1(t_0)\Delta t + \frac{1}{2}\mathbf{a}_2(t_0)\Delta t^2 \tag{12}$$

$$\mathbf{r} \approx \mathbf{r}_0 + \dot{\mathbf{r}}_0\Delta t + \frac{1}{2}\mathbf{a}_1(t_0)\Delta t^2 + \frac{1}{6}\mathbf{a}_2(t_0)\Delta t^3 \tag{13}$$

Finally, the attitude with respect to the inertial frame is propagated forward in time using the compensated gyro measurement. The IMU case-to-inertial attitude quaternion at time $t_{k,j}$ is denoted as $\mathbf{q}_{c\to i}(t_{k,j})$, the quaternion is simply propagated with the quaternion multiplication

$$\mathbf{q}_{c\to i}(t_{k,j+1}) = \Delta\mathbf{q}_c(t_{k,j+1}) \cdot \mathbf{q}_{c\to i}(t_{k,j}) \tag{14}$$

where $\Delta\mathbf{q}_c(t_{k,j+1})$ is the change in attitude from the current IMU case frame to the prior IMU frame, which is simply the opposite of the latest gyro measurement expressed as a quaternion. Notice that the gyro measurement is sample internally by the sensor at a very high rate and compensated for coning errors, therefore this propagation scheme is very accurate. The propagated Orion body attitude $\mathbf{q}_{i\to b}(t_{k,j+1})$ is simply obtained from the fixed IMU case to Orion body transformation

$$\mathbf{q}_{i\to b}(t_{k,j+1}) = \mathbf{q}_{c\to i}(t_{k,j+1})^* \cdot \mathbf{q}_{c\to b} \tag{15}$$

where the superscript "$*$" indicates the quaternion conjugate. Notice that the mounting error of the IMU with respect to the Orion body is unknown, therefore $\mathbf{q}_{b\to i}$ contains that additional error.

B. State Propagation

When FiltNav receives new EKF data, it updates its estimates of the IMU errors used for measurement compensation, resets the 4 Hz buffers, and updates its position, velocity, and quaternion states with the information from the filter. The EKF provides a state update (or delta state $\Delta\mathbf{X}$) which is one major cycle (nominally one second) in the past. Following standard linearization techniques, the delta state is propagated forward by the state transition matrix that FiltNav needs to calculate. The change in state $\mathbf{X}$ at time t_k is obtained from a change in state at time t_{k-1} as

$$\Delta\mathbf{X}_k = \mathbf{\Phi}(t_k, t_{k-1})\Delta\mathbf{X}_{k-1} \tag{16}$$

the nonlinear state dynamics is $\dot{\mathbf{X}} = \mathbf{F}(\mathbf{X}, t)$, its Jacobian is

$$\mathbf{A}(t_k) = \left.\frac{\partial\mathbf{F}}{\partial\mathbf{X}}\right|_{\mathbf{X}_k=\hat{\mathbf{X}}_k}(t_k) \tag{17}$$

and the State Transition Matrix (STM) evolves as

$$\dot{\mathbf{\Phi}}(t, t_{k-1}) = \mathbf{A}(t)\mathbf{\Phi}(t, t_{k-1}) \tag{18}$$

Since FiltNav operates at a fairly high rate, a first order approximation of the STM was used since sufficiently accurate to represent the dynamics, hence (the low rate EKF uses a higher order approximation)

$$\mathbf{\Phi}(t_{k+1}, t_{k-1}) \simeq \mathbf{\Phi}(t_k, t_{k-1}) + \mathbf{A}(t_k)\mathbf{\Phi}(t_k, t_{k-1})\,(t_{k+1} - t_k) \tag{19}$$

hence the need to multiply the Jacobian matrix $\mathbf{A}$ and the state transition matrix $\mathbf{\Phi}$, this multiplication is done taking advantage of the known form of the two matrices.

The IMU error states are modeled as first-order Gauss Markov states, which are denoted as $\mathcal{B}$, so that the state-space is

$$\mathbf{X} \;=\; \begin{bmatrix} \mathbf{x}^{\mathrm{T}} & \boldsymbol{\phi}_{i_{ref}}^{i^T} & \mathcal{B}^T \end{bmatrix}^T \tag{20}$$

where $\mathbf{x}$ is the 6×1 vector containing inertial position and velocity, the three dimensional multiplicative attitude error [15] $\boldsymbol{\phi}_{i_{ref}}^{i}$ is coordinated in the inertial frame rather than the Orion body frame for reasons that will be soon clear. Matrix $\mathbf{A}(t_k)$ is partitioned as follows

$$\mathbf{A}(t_k) = \begin{bmatrix} \mathbf{A}_{\mathbf{xx}}(t_k) & \mathbf{A}_{\mathbf{x}\boldsymbol{\phi}}(t_k) & \mathbf{A}_{\mathbf{x}\mathcal{B}}(t_k) \\ \mathbf{0} & \mathbf{A}_{\boldsymbol{\phi}\boldsymbol{\phi}}(t_k) & \mathbf{A}_{\boldsymbol{\phi}\mathcal{B}}(t_k) \\ \mathbf{0} & \mathbf{0} & \mathbf{A}_{\mathcal{B}\mathcal{B}}(t_k) \end{bmatrix} \tag{21}$$

Since the elements of $\mathcal{B}$ are modeled as independent first-order Gauss-Markov processes, $\mathbf{A}_{\mathcal{B}\mathcal{B}}(t_k)$ is diagonal. Dropping all time dependencies for simplicity, the state transition matrix, $\mathbf{\Phi}$, can be partitioned, likewise, as

$$\mathbf{\Phi}(t_k, t_{k-1}) = \begin{bmatrix} \mathbf{\Phi}_{\mathbf{xx}} & \mathbf{\Phi}_{\mathbf{x}\boldsymbol{\phi}} & \mathbf{\Phi}_{\mathbf{x}\mathcal{B}} \\ \mathbf{0} & \mathbf{\Phi}_{\boldsymbol{\phi}\boldsymbol{\phi}} & \mathbf{\Phi}_{\boldsymbol{\phi}\mathcal{B}} \\ \mathbf{0} & \mathbf{0} & \mathbf{\Phi}_{\mathcal{B}\mathcal{B}} \end{bmatrix} = \begin{bmatrix} \mathbf{\Phi}_{\mathbf{x}\mathbf{X}} \\ \mathbf{\Phi}_{\boldsymbol{\phi}\mathbf{X}} \\ \mathbf{\Phi}_{\mathcal{B}\mathbf{X}} \end{bmatrix} \tag{22}$$

and it follows that

$$\mathbf{A}(t_k)\mathbf{\Phi}(t_k, t_{k-1}) = \begin{bmatrix} \mathbf{A}_{\mathbf{xx}}\mathbf{\Phi}_{\mathbf{xx}} & (\mathbf{A}_{\mathbf{xx}}\mathbf{\Phi}_{\mathbf{x}\boldsymbol{\phi}} + \mathbf{A}_{\mathbf{x}\boldsymbol{\phi}}\mathbf{\Phi}_{\boldsymbol{\phi}\boldsymbol{\phi}}) & (\mathbf{A}_{\mathbf{xx}}\mathbf{\Phi}_{\mathbf{x}\mathcal{B}} + \mathbf{A}_{\mathbf{x}\boldsymbol{\phi}}\mathbf{\Phi}_{\boldsymbol{\phi}\mathcal{B}} + \mathbf{A}_{\mathbf{x}\mathcal{B}}\mathbf{\Phi}_{\mathcal{B}\mathcal{B}}) \\ \mathbf{0} & \mathbf{A}_{\boldsymbol{\phi}\boldsymbol{\phi}}\mathbf{\Phi}_{\boldsymbol{\phi}\boldsymbol{\phi}} & (\mathbf{A}_{\boldsymbol{\phi}\boldsymbol{\phi}}\mathbf{\Phi}_{\boldsymbol{\phi}\mathcal{B}} + \mathbf{A}_{\boldsymbol{\phi}\mathcal{B}}\mathbf{\Phi}_{\mathcal{B}\mathcal{B}}) \\ \mathbf{0} & \mathbf{0} & \mathbf{A}_{\mathcal{B}\mathcal{B}}\mathbf{\Phi}_{\mathcal{B}\mathcal{B}} \end{bmatrix} \tag{23}$$

The reason to choose the attitude deviation $\boldsymbol{\phi}^i_{i_{ref}}$ expressed in the inertial frame is that produces $\mathbf{A}_{\phi\phi} = \mathbf{0}$, which results in a state transition matrix with the following form

$$\boldsymbol{\Phi}(t_k, t_{k-1}) = \begin{bmatrix} \boldsymbol{\Phi}_{\mathbf{xx}} & \boldsymbol{\Phi}_{\mathbf{x}\phi} & \boldsymbol{\Phi}_{\mathbf{x}\mathcal{B}} \\ \mathbf{0} & \mathbf{0} & \boldsymbol{\Phi}_{\phi\mathcal{B}} \\ \mathbf{0} & \mathbf{0} & \boldsymbol{\Phi}_{\mathcal{B}\mathcal{B}} \end{bmatrix} \tag{24}$$

The gyro errors are updated directly and assumed constant during the one second FiltNav propagation in between major cycles, hence computation of $\boldsymbol{\Phi}_{\mathcal{B}\mathcal{B}}$ and the entire rows of the state transition matrix associated with it are not needed, since only position, velocity and attitude are updated.

The attitude update in FiltNav is given by

$$\boldsymbol{\phi}^i_{i_{ref}}(t_k) = \boldsymbol{\phi}^i_{i_{ref}}(t_{k-1}) + \boldsymbol{\Phi}_{\phi\mathcal{B}}(t_k, t_{k-1})\Delta\mathcal{B}_{k-1} \tag{25}$$

It is noticed that the attitude update at time t_k is dominated by $\boldsymbol{\phi}^i_{i_{ref}}(t_{k-1})$ and therefore the second component of Eq. (25) is dropped to save the computations of calculating the state transition matrix. In summary, FiltNav receives an inertial attitude update already parameterized as a delta quaternion $\Delta\mathbf{q}_i(t_{k-1})$ and it updates its current estimate of attitude using the quaternion composition rule

$$\hat{\mathbf{q}}^+_{i\to b}(t_k) = \Delta\mathbf{q}_i(t_{k-1}) \cdot \hat{\mathbf{q}}^-_{i\to b}(t_k) \tag{26}$$

while position and velocity are simply updated as

$$\hat{\mathbf{x}}^+_k = \hat{\mathbf{x}}^-_k + \boldsymbol{\Phi}_{\mathbf{xX}}(t_k, t_{k-1})\Delta\mathbf{X}_{k-1} \tag{27}$$

where $\boldsymbol{\Phi}_{\mathbf{xX}}(t_k, t_{k-1})$ is defined in Eq. (22).

IV. Extended Kalman Filter Design

The Extended Kalman Filter is a 1 Hz CSU responsible for incorporating the measurements into the filtered navigator solution.

The state vector components are divided in dynamic-states, $\mathcal{X}$ and parameter-states, $\mathcal{B}$

$$\mathbf{X} \;=\; \begin{bmatrix} \mathcal{X}^T & \mathcal{B}^T \end{bmatrix}^T \tag{28}$$

Table 1 show the 35 states of the EFT-1 EKF. The 24 IMU states are included in the EKF as parameter-states and they differ from the other 11 states in that they are modeled as independent

first-order Markov processes, therefore their time evolution is known analytically and does not necessitate numerical integration. In addition, their state transition matrix is also known analytically and it is very sparse, making their covariance matrix propagation extremely numerically efficient.

Table 1 EKF States

State	# of elements	Comments/Description
Position	3	3-vector of inertial frame components of position
Velocity	3	3-vector of inertial frame components of velocity
Attitude	3	Multiplicative Attitude deviation state
Clock Bias and Drift	2	GPS receiver clock states
accel bias	6	3 states each for low-g and high-g accelerometer modes
accel scale factor	3	
accel misalignment	6	includes both internal misalignment and non-orthogonality
gyro bias	3	
gyro scale factor	3	
gyro non-orthogonality	3	the gyro is taken as the aligned sensor

The EKF's covariance is factorized using the UDU formulation, which has been successfully used in aerospace engineering applications for several decades. Orion utilizes the UDU factorization since it is very numerically stable. The UDU formulation factors the covariance matrix (which is symmetric) as

$$\mathbf{P} = \mathbf{UDU}^T \tag{29}$$

where $\mathbf{U}$ is a 35×35 Upper triangular matrix which has 1's on the diagonal and $\mathbf{D}$ is an 35×35 Diagonal matrix.

A. The Propagation Phase

The time propagation of position, velocity, and attitude was previously discussed and occurs in FiltNav. Accelerometer editing (or thresholding [9]) is included in the EKF design but it was disabled. Accelerometer editing consists in using the accelerometer measurement to propagate the state

only when it exceeds a predetermined threshold. The threshold is determined from the accelerometer's specification, the idea is not to include the measurement when most of what is measured is just sensor error. When the measurement is below the threshold, the EKF is capable of performing its own propagation independent of FiltNav. As a cost-saving measure, the inclusion of the low-g mode was eliminated from the EFT-1 IMU design, therefore the IMU provided a coarse measurement during the orbital phase originally intended only for the highly dynamic atmospheric phases. During EFT-1, Orion was attached to the upper stage for most of the orbital flight, venting from the large upper stage engine was significant and below the threshold, producing large accumulated position and velocity errors. Therefore the accelerometer threshold was set to zero and all accelerometer measurements were included in the state propagation.

The efficiency and robustness of the UDU formulation have been harnessed in the time-update of the covariance matrix. To propagate the covariance the State Transition Matrix is calculated. Integrating the STM and computing the propagated covariance with the discrete propagation formula is usually more computationally efficient than integrating the covariance Riccati equation directly, since the STM usually has a known sparse structure and can be often approximated with a truncated matrix exponential. This offers particular advantages in the case of the Orion Absolute Navigation Filters since the majority of the states are independent first-order Gauss-Markov states and their state transition matrix is expressed analytically. Additionally, the STM for the GPS clock states is also known analytically. The UDU covariance propagation relies on a very efficient "rank one update" algorithm derived by Agee and Turner [6].

Process noise is used to tune the filter. For the Orion Absolute Navigation Filter, the process noise enters the covariance update via the dynamic states and the parameter states. For the position and velocity, the process noise enters via the velocity state; the process noise represents the uncertainty in the dynamics, chiefly caused by mis-modeled (or unmodeled) accelerations. Since the accelerometers only measure non-inertial forces, gravity is modeled via a high-order gravity model. For the Orion Absolute Navigation filter, Earth's gravity is modeled by an 8×8 gravity field; higher-order spherical harmonics are neglected and hence are captured by the velocity process noise. Additionally, since the attitude rate states are not part of the filter, the attitude process noise

enters via the gyro angle random walk. The velocity and attitude process noises are obtained from the IMU Velocity Random Walk and Angular Random Walk performance, respectively. Conservative values of 0.96741 ft^2/s and 0.0096741ft^2/s^3 are used for the clock bias and drift process noise, respectively. These values are looser than the receiver's clock specifications.

The IMU states are modeled as first-order Gauss-Markov processes and carry with them corresponding process noise parameters which are used in the tuning of the filter. Since the IMU errors were expected to be quite constant during the 4.5 hour flight, the time constant of these parameters was chosen as 4 hours, and the process noise was chosen such that the steady-state value of the Markov processes was equal to the vendor's specification.

B. The Measurement Update

As is routinely done, measurements are processed one-at-a-time. The performance of an EKF is dependent on the order in which one processes measurements [16]. The Orion EKF design obviates this fact by calculating all the measurement Jacobians at once with the *a priori* estimate and simply calculating a delta state update and only applying it to update the state once all the measurements at a given time are processed. The state update is accumulated in the quantity $\Delta\mathbf{X}$ and it can be shown that this approach is mathematically equivalent to an extended Kalman Filter that employs a vector update to process all new measurements at once.

Evaluating the performance of GPSR was one of the EFT-1 objectives, and the EKF was purposefully tuned to be conservative in processing PR and DR measurements. The measurement standard deviations for PR and DR used in the filter are 60 ft and 3 ft, respectively, which are large enough numbers that the inclusion of satellite specific bias states was not necessary. The PR 60 ft value is actually a lower limit, a GPSR outputted value is used instead when this value exceeds 60 ft. The GPSR estimate of the measurement uncertainty contains the estimate of all errors (including atmospheric delays) except receiver clock errors. However, since atmospheric delays become significant for low-elevation satellites making the measurement error very strongly autocorrelated, these low-elevation satellites' measurements were not included in the filter. Because of the large range of altitudes at which GPSR operates during this flight, it is not possible to use a

constant masking angle to exclude low-elevation satellites. Fig. 3 shows the approach used to mask low-elevation satellites. The elevation angle θ is calculated from the Orion position vector $\mathbf{R}_1$ and the line-of-sight vector from Orion to the GPS Satellite $\mathbf{R}_2$ as

$$\cos\theta = -(\mathbf{R}_1 \cdot \mathbf{R}_2)/(\|\mathbf{R}_1\| \, \|\mathbf{R}_2\|) \tag{30}$$

$$\sin\theta = \|\mathbf{R}_1 \times \mathbf{R}_2\|/(\|\mathbf{R}_1\| \, \|\mathbf{R}_2\|) \tag{31}$$

The point of closest approach (PCA) is given by

$$PCA = \|\mathbf{R}_1\| \, \sin\theta \tag{32}$$

the satellite is masked when PCA is below a user-defined threshold and $\cos\theta$ is positive, this second condition protects against masking good signals when the Orion position is the point of closest approach ($\theta > \pi/2$), (see right-hand side of Fig. 3).

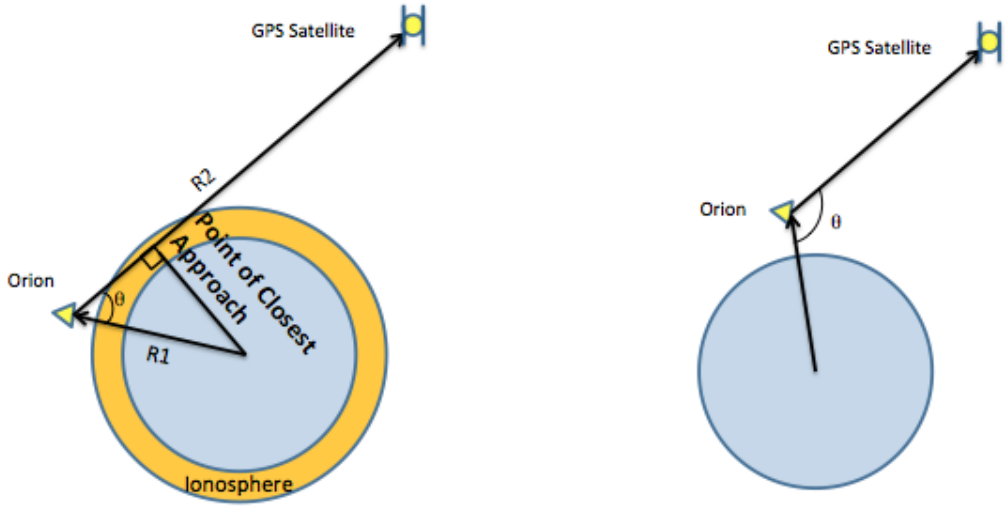

Fig. 3 GPS Satellites low-elevation Masking

a. Dealing with Measurement Latency In general, the measurement time tags are not going to be equal to the current filter epoch time, t_k. To state it another way, the measurements do not come in at the current time. Thus, a situations arises where the filter has propagated its state and covariance to time $t = t_k$ from time $t = t_{k-1}$, and is subsequently given a measurement to be filtered (denoted by subscript m) that corresponds to the time $t = t_m$, where

$$t_m \leq t_k \tag{33}$$

If $\Delta t = t_m - t_k$ is not insignificant, the time difference between the measurement and the filter state and covariance will need to be accounted for during filtering in order to accurately process the measurement. This can be done in much the same way a batch filter operates (see pages 196-197 of Tapley [10]). If the measurement at time $t = t_m$ is denoted as y_m, the filter state at that time is given by $\hat{\mathbf{x}}_m \equiv \hat{\mathbf{x}}(t_m)$, and the measurement model is denoted as $h\left(\mathbf{x}_m, t_m\right)$, then one can expand the measurement model to first-order about the nominal filter state to get

$$h\left(\mathbf{x}_m, t_m\right) = h\left(\hat{\mathbf{x}}_m, t_m\right) + \widetilde{\mathbf{H}}_m \delta\mathbf{x}_m \tag{34}$$

where $\delta\mathbf{x}_m = \mathbf{x}_m - \hat{\mathbf{x}}_m$ and $\widetilde{\mathbf{H}}_m$ is defined as

$$\widetilde{\mathbf{H}}_m = \left(\frac{\partial h\left(\mathbf{X}, t_m\right)}{\partial \mathbf{X}}\right)_{\mathbf{x}=\hat{\mathbf{x}}_m} \tag{35}$$

The perturbed state at time t_m, $\mathbf{x}_m$ can be written in terms of the state at time t_k via state propagation as follows

$$\delta\mathbf{x}_m = \mathbf{\Phi}(t_m, t_k)\delta\mathbf{x}_k + \mathbf{\Gamma}_m \boldsymbol{\nu}_m \tag{36}$$

where $\boldsymbol{\nu}_m$ is process noise, so the measurement is computed as

$$h\left(\mathbf{x}_m, t_m\right) = h\left(\hat{\mathbf{x}}_m, t_m\right) + \widetilde{\mathbf{H}}_m \mathbf{\Phi}(t_m, t_k)\delta\mathbf{x}_k + \widetilde{\mathbf{H}}_m \mathbf{\Gamma}_m \boldsymbol{\nu}_m \tag{37}$$

the state process noise from $t = t_m$ to $t = t_k$ has the characteristics $E[\boldsymbol{\nu}_m] = \mathbf{0}$ and $E[\boldsymbol{\nu}_m \boldsymbol{\nu}_m^T] = \mathbf{Q}_m$. Additive measurement noise is added with characteristics $E[\eta_m] = 0$ and $E[\eta_m^2] = R_m$.

Upon taking the conditional expectation of the measurement equation and rearranging, the scalar residual ϵ_m of the measurement is given by

$$\epsilon_m = y_m - h(\hat{\mathbf{x}}_m, t_m) = \widetilde{\mathbf{H}}_m \delta\mathbf{x}_m + \eta_m = \widetilde{\mathbf{H}}_m \mathbf{\Phi}(t_m, t_k)\delta\mathbf{x}_k + \widetilde{\mathbf{H}}_m \mathbf{\Gamma}_m \boldsymbol{\nu}_m + \eta_m \tag{38}$$

The measurement partials that are used in the update, which map the measurement at time t_m to the state at time $t = t_k$, are given by

$$\mathbf{H}_m = \widetilde{\mathbf{H}}_m \mathbf{\Phi}(t_m, t_k) \tag{39}$$

From the above discussion, it is evident that the quantities needed to update the state at time $t = t_k$ with a measurement from time $t = t_m$ are the nominal state back-propagated to the

measurement time, $\hat{\mathbf{x}}_m$, and the state transition matrix relating the two times, $\mathbf{\Phi}(t_m, t_k)$. Given these values, $h\left(\hat{\mathbf{x}}_m, t_m\right)$ and $\mathbf{H}_m$ can be calculated and used to update state and covariance.

The nominal state at the measurement time is calculated by back-propagating the filter state from time t_k to time t_m at 4 Hz using buffered IMU data from FiltNav. The same 4Hz buffers are used to back propagate the transition matrix. The same propagation algorithms used in forward propagation are utilized for the back-propagation, with the exception that the smaller time step allows for a first-order approximation of the matrix exponential used to update the state transition matrix. Notice that the first order approximation did break under the parachutes due to very high rotational dynamics, to mitigate this fact, measurement processing was inhibited in EFT-1 during high dynamics phases.

Measurement Underweighting Measurement underweighting has long been standard practice in human-rated on-board navigation since Apollo [11]. This is used in lieu of a second-order measurement update which is used in the so-called second-order EKF, which is more computationally expensive. Underweighting is needed when accurate measurements (such as GPS) are introduced at a time when the *a priori* covariance (particularly of the position and velocity states) matrix is large. In the case of GPS measurements, the update to the position and velocity states would result in the covariance matrix associated with these states 'clamping' down too fast, resulting in an unrealistically small uncertainty compared to the actual covariance matrix. This undesired behavior can result in rejection of subsequent valid measurements. The underweighting factor decreases the rate at which the covariance decreases, essentially approximating the second-order terms of the Taylor series which are not explicitly included in the EKF. Underweighting is typically implemented during the Kalman Gain calculation by

$$\mathbf{K}_k = \mathbf{P}_k \mathbf{H}_k^T \Big((\alpha + 1) \mathbf{H}_k \mathbf{P}_k \mathbf{H}_k^T + R_k \Big)^{-1}$$

However, the implementation is complicated when using the UDU formulation described earlier in this paper. The Orion team has implemented a simple new formulation to allow this. It is observed that the effect of underweighting can also be described as simply an additional measurement noise. In the Orion EKF, the underweighting correction is simply added to the measurement noise prior

to the UDU update.

$$R_{UW_k} \;=\; R_k + \alpha \mathbf{H}_k \mathbf{P}_k \mathbf{H}_k^T$$

Thus, the result of applying underweighting adds robustness to cases where relatively accurate measurement updates are processed in the presence of large navigation errors and large uncertainties.

EFT-1 employed a coefficient of 0.2 on both PR and DR, and underweighting was applied when $\mathbf{H}_k \mathbf{P}_k \mathbf{H}_k^T > 10,000 \text{ ft}^2$ for any given measurement.

Measurement Editing The Kalman filter state update is the linear combination of two components, the prior estimate $\hat{\mathbf{X}}_k^-$ and the measurement residual $\big(\mathbf{y}_k - \mathbf{h}(\hat{\mathbf{x}}_k^-)\big)$

$$\hat{\mathbf{x}}_k^+ = \hat{\mathbf{x}}_k^- + \mathbf{K}_k\big(\mathbf{y}_k - \mathbf{h}(\hat{\mathbf{x}}_k^-)\big) \tag{40}$$

The measurement residual is the difference between the actual measurement $\mathbf{y}$ and the value of the measurement as predicted by the filter, $\mathbf{h}(\hat{\mathbf{x}}^-)$. The larger the residual, the larger the discrepancy between the actual measurement and the filter's prediction of it, and as a consequence the larger the measurement update. The residual is scaled by the Kalman gain $\mathbf{K}$, which for a scalar measurement is given by

$$\mathbf{K}_k = \frac{\mathbf{P}_k \mathbf{H}_k^T}{\mathbf{H}_k \mathbf{P}_k \mathbf{H}_k^T + R_k} = \frac{\mathbf{P}_k \mathbf{H}_k^T}{W_k} \tag{41}$$

where W is the residual variance. When the measurements are linear W corresponds exactly to the variance of the residual. From Eq. (41), it follows that the larger the uncertainty of the prior state ($\mathbf{P}$), the larger the update, conversely, the larger the uncertainty of the residual W, the smaller the update.

Knowledge of the residual and its expected variance by the filter allows monitoring of their consistency. In Orion, a measurement is rejected if the residual does not lie within 5 times its predicted standard deviation (square root of the variance), where 5 is a tunable, user-defined parameter. Few failures indicate an occasional bad measurement, while repeated rejections indicate a sensor failure or filter divergence.

Consider Covariance and It's Implementation in the UDU Filter The Consider Kalman Filter, also called the Schmidt-Kalman Filter is especially useful when parameters have

low observability.

Any state except position, velocity, and clock errors can be considered rather than estimated in the Orion EKF. In order to describe how consider states are incorporated the state-vector $\mathbf{X}_k$ is partitioned into the $n_\mathbf{s}$"estimated states", $\mathbf{s}$, and the $n_\mathbf{p}$ "consider" parameters, $\mathbf{p}$. It is important to distinguish the "consider parameters" in this section from the "parameter state" in the filter design. A consider parameter is simply an element of the EKF state that is propagated only. It is not updated with the measurement; its effect is only considered. As previously explained, a parameter state is simply a state modeled as a first-order Markov process. Every dynamic state or parameter state is allowed to be considered with the exception of position and velocity. Hence for the purpose of this discussion, the state vector (including both dynamic states and parameter states) is partitioned as:

$$\mathbf{X}_k^{\mathrm{T}} = \begin{bmatrix} \mathbf{s}_k^{\mathrm{T}} & \mathbf{p}_k^{\mathrm{T}} \end{bmatrix} \tag{42}$$

subscripts k indicating the time step are omitted for the rest of this section for ease of notation, the estimation error covariance matrix can be similarly partitioned

$$\mathbf{P} = \begin{bmatrix} \mathbf{P_{ss}} & \mathbf{P_{sp}} \\ \mathbf{P_{ps}} & \mathbf{P_{pp}} \end{bmatrix}, \quad \mathbf{H} = \begin{bmatrix} \mathbf{H_s} & \mathbf{H_p} \end{bmatrix}, \quad \mathbf{K}_{opt} = \begin{bmatrix} \mathbf{K}_{\mathbf{s},opt} \\ \mathbf{K}_{\mathbf{p},opt} \end{bmatrix} = \begin{bmatrix} \mathbf{P_{ss}^- H_s^T} + \mathbf{P_{sp}^- H_p^T} \\ \mathbf{P_{ps}^- H_s^T} + \mathbf{P_{pp}^- H_p^T} \end{bmatrix} \mathbf{W}^{-1}$$

where $\mathbf{K}_{opt}$ is the optimal Kalman gain computed for the full state, $\mathbf{X}$. Therefore, choosing $\mathbf{K_s}$ such that $\mathbf{K_s} = \mathbf{K}_{\mathbf{s},opt}$ and $\mathbf{K_p}$ arbitrary, the *a posteriori* covariance matrix is [8]

$$\mathbf{P}^+ = \begin{bmatrix} \mathbf{P_{ss}^- - K_s W K_s^T} & \mathbf{P_{sp}^- - K_s H} \begin{bmatrix} \mathbf{P_{sp}^-} \\ \mathbf{P_{pp}^-} \end{bmatrix} \\ \mathbf{P_{ps}^-} - \begin{bmatrix} \mathbf{P_{sp}^-} \\ \mathbf{P_{pp}^-} \end{bmatrix}^T \mathbf{H}^T \mathbf{K_s^T} & \mathbf{P_{pp}^- - K_p W K_p^T} \end{bmatrix} \tag{43}$$

This equation is valid for any value of $\mathbf{K_p}$. Notice that there is no $\mathbf{K_p}$ in the off-diagonal blocks (correlation terms) of the covariance matrix. Therefore, what is remarkable about this equation is that once the optimal $\mathbf{K_s}$ is chosen, the correlation between $\mathbf{s}$ and $\mathbf{p}$ is independent of the choice of $\mathbf{K_p}$.

In its essence, the consider parameters are not updated; therefore, the Kalman gain associated with the consider parameters, $\mathbf{p}$, is zero, *i.e.* $\mathbf{K_p} = \mathbf{0}$

1. When using the Schmidt-Kalman filter, the *a priori* and *a posteriori* covariance of the parameters ($\mathbf{P_{pp}}$) are the same.

2. The *a posteriori* covariance matrix of the states and the correlation between the states and the parameters are the same regardless of whether one uses the Schmidt-Kalman filter or the optimal Kalman update

Therefore, the *consider* covariance, $\mathbf{P}^+_{con}$ is

$$\mathbf{P}^+_{con} = \begin{bmatrix} \mathbf{P^-_{ss}} - \mathbf{K_s W K_s}^T & \mathbf{P^-_{sp}} - \mathbf{K_s H} \begin{bmatrix} \mathbf{P^-_{sp}} \\ \mathbf{P^-_{pp}} \end{bmatrix} \\ \mathbf{P^-_{ps}} - \begin{bmatrix} \mathbf{P^-_{sp}} \\ \mathbf{P^-_{pp}} \end{bmatrix}^T \mathbf{H}^T \mathbf{K}_\mathbf{s}^T & \mathbf{P^-_{pp}} \end{bmatrix} \tag{44}$$

Of course, the "full" optimal covariance matrix update is

$$\mathbf{P}^+_{opt} = \begin{bmatrix} \mathbf{P^-_{ss}} - \mathbf{K_{s,}}_{opt} \mathbf{W K_{s,}}_{opt}^T & \mathbf{P^-_{sp}} - \mathbf{K_{s,}}_{opt} \mathbf{H} \begin{bmatrix} \mathbf{P^-_{sp}} \\ \mathbf{P^-_{pp}} \end{bmatrix} \\ \mathbf{P^-_{ps}} - \begin{bmatrix} \mathbf{P^-_{sp}} \\ \mathbf{P^-_{pp}} \end{bmatrix}^T \mathbf{H}^T \mathbf{K}_{\mathbf{s},opt}^T & \mathbf{P^-_{pp}} - \mathbf{K_{p,}}_{opt} \mathbf{W K_{p,}}_{opt}^T \end{bmatrix} \tag{45}$$

The UDU formulation, while numerically stable and tight, is quite inflexible to making any changes in the framework. The measurement update, expressed in terms of the consider covariance [8], is

$$\mathbf{P}^+_{opt} = \mathbf{P}^+_{con} - W \left(\mathbf{S K}_{opt}\right) \left(\mathbf{S K}_{opt}\right)^T \tag{46}$$

where $\mathbf{S}$ is an $n_\mathbf{x} \times n_\mathbf{x}$ matrix (defining $n_\mathbf{x} = n_\mathbf{s} + n_\mathbf{p}$, where $n_\mathbf{x}$ is the total number of states, $n_\mathbf{p}$ is the number of consider states, and $n_\mathbf{s}$ is the number of "non-consider" states) defined as

$$\mathbf{S} = \begin{bmatrix} \mathbf{0}_{n_\mathbf{s} \times n_\mathbf{s}} & \mathbf{0}_{n_\mathbf{s} \times n_\mathbf{p}} \\ \mathbf{0}_{n_\mathbf{p} \times n_\mathbf{s}} & \mathbf{I}_{n_\mathbf{p} \times n_\mathbf{p}} \end{bmatrix} \tag{47}$$

Since scalar measurements are processed, $W = 1/\alpha$ is a scalar and $\mathbf{K}_{opt}$ is an $n_\mathbf{x} \times 1$ vector. Therefore $\mathbf{SK}_{opt}$ is an $n_\mathbf{x} \times 1$ vector. Therefore, solving for the consider covariance,

$$\mathbf{P}^+_{con} = \mathbf{P}^+_{opt} + W \left(\mathbf{S K}_{opt}\right) \left(\mathbf{S K}_{opt}\right)^T \tag{48}$$

Eq. (46) has the same form as the original rank-one update *i.e.* $\mathbf{P}^+ = \mathbf{P}^- + c\mathbf{a}\mathbf{a}^T$ hence the Agee-Turner rank one update is used.

Therefore, the procedure is as follows: first perform a complete rank-one measurement update with the optimal Kalman Gain ($\mathbf{K}_{opt}$) with the Carlson rank-one update on the full covariance matrix. Second, perform another rank-one update with $\mathbf{a} = \mathbf{S}\mathbf{K}_{opt}$ and $c = W$, according to the Agee-Turner rank-one update. While this capability exists in the Orion navigation flight software, it was not used in EFT-1.

V. Absolute Navigation Performance

This section shows the onboard navigation telemetry data from the EFT-1 flight. At various points during the flight Orion was tracked from ground stations, and the solution was evaluated by mission control to verify the performance of the onboard navigation system. All these checks compared very favorably to the onboard solution, demonstrating good performance. The ground navigation measurements were combined with all the GPS measurements into a Kalman smoother to obtain a Best Estimated Trajectory (BET) of EFT-1 [12]. The overall performance of the onboard navigation solution compared to the BET is shown in Ref. [13]. Through comparison with the ground tracking solutions during flight, with the navigation performance obtained in many Monte Carlo simulations, and through monitoring of the GPSR residuals, it can be inferred with a high degree of confidence that the EKF's predicted performance (i.e. estimation error covariance) during low-elevation is a good indicator of the actual (unknowable) estimation error experienced during flight. All plots show the performance of channel one (CH1) and channel two (CH2) produced very similar results.

Figure 4 shows the EKF position covariance throughout the flight. The estimates are typically within 50 ft (3σ) during coasting flight, and exhibit nominal growth and re-convergence during the brief measurement outage caused by Orion's reorientation to its upper stage separation (CMsep) attitude (around 12,000 seconds of mission time). Nominal convergence occurred at GPSR acquisition during ascent (around 400 sec) and the position uncertainty grew very fast during the high dynamic entry when GPSR measurements were inhibited because of high rates under the chutes

(past 15,000 sec).

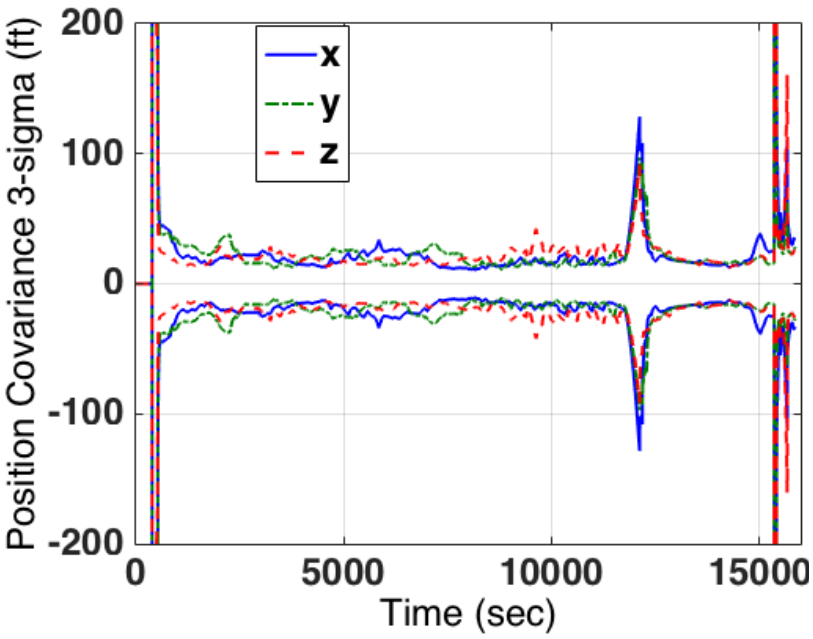

Fig. 4 CH1 ECI Position Covariance 3σ

Figure 5 shows similar trends for the EKF velocity covariance. The estimates are typically bounded within 0.3 ft/s (3σ) during coasting flight, and exhibit nominal growth and re-convergence during the second stage burn (∼7,000 sec) and the brief outage caused by the CMsep attitude. The velocity covariance also grows fast during GPSR outages during entry.

In order to confirm that the filter re-converged properly after measurement outages, the best indicator are the residuals shown in Figure 6 for both pseudorange and delta range, the residuals of all measurements processed are shown together, the bottom sub-plot shows the total number of pseudorange measurements available. After each outage, the residuals start significantly larger and then re-converge to the smaller values. GPSR performed very well during the flight [14], and proved to be very reliable tracking satellites all the way through apogee. After the outage due to CMsep, the residuals jump to 400 ft, almost entirely a combination of the receiver clock bias error and the position estimation error. Figure 7 shows the covariance of the clock bias and drift states.

Figure 8 shows the pseudorange and delta range measurement residuals scaled by the filter's predicted standard deviation. It can be seen that the predictions are conservative compared to the actual residuals, as the PR residuals go outside 1 σ predictions only once after blackout and they

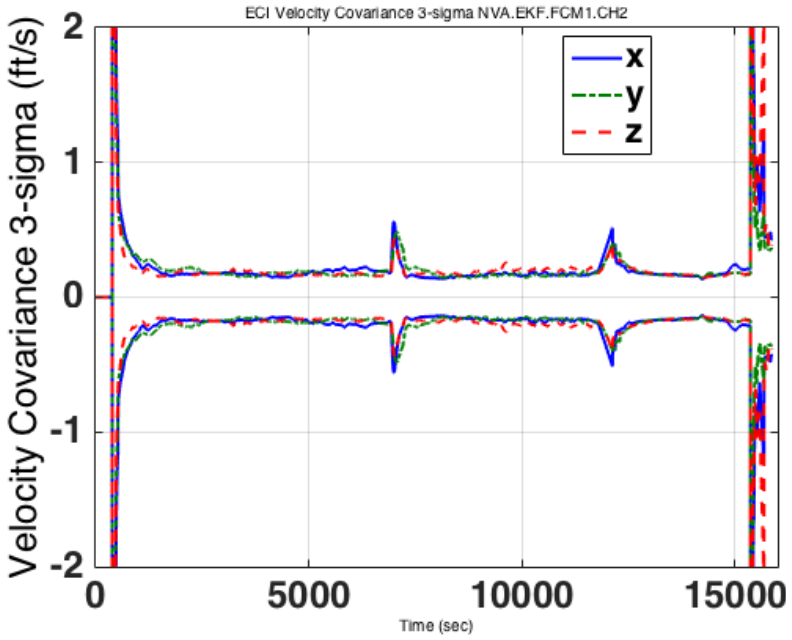

Fig. 5 CH1 ECI Velocity Covariance 3σ

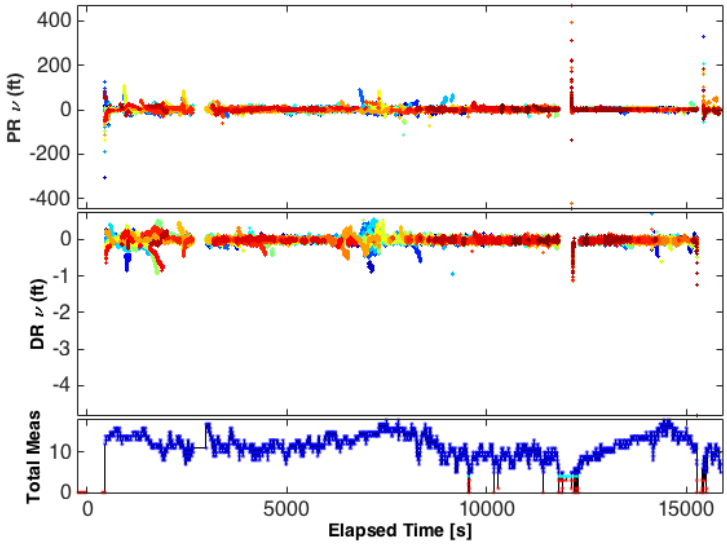

Fig. 6 CH1 Pseudorange Residuals

almost always are below 0.5 σ, and the rejection threshold is 5 σ. The DR residuals are tuned even more conservatively, as they always stay below 0.3 σ. This feature was expected and the performance was as intended. This design choice is due to the desire to test the new GPS receiver with the mission. The GPSR estimate of the pseudorange uncertainty was used unless a value below 60 ft was output. The receiver produced conservative estimates of the errors that included errors

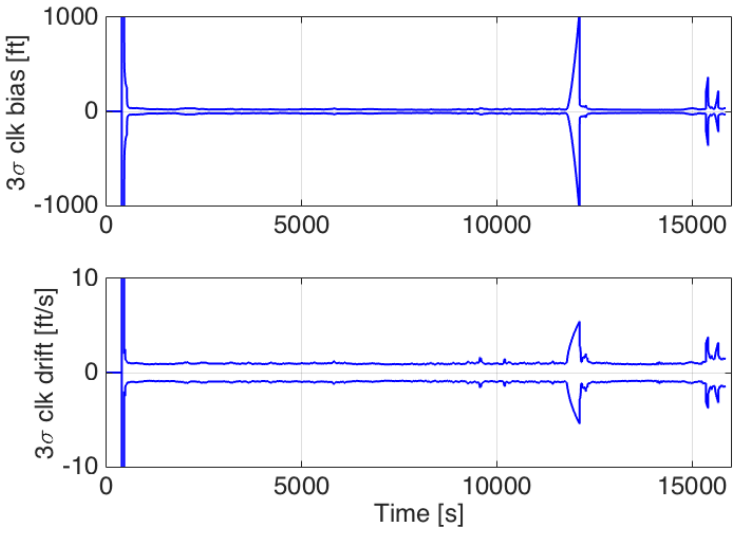

Fig. 7 CH1 Clock Bias and Drift Covariance 3σ

due to atmospheric delay.

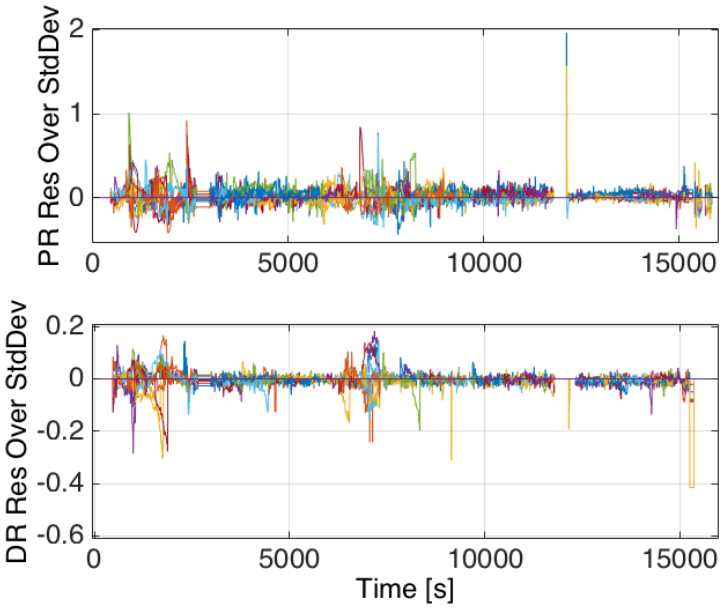

Fig. 8 CH1 PR and DR Residuals Scaled by Predicted Standard Deviation

Figure 9 shows very good attitude performance throughout the flight even in the absence of a dedicated attitude sensor. Attitude is observable via the dynamics measured by the accelerometer in the body frame and the GPSR antennas lever arm with respect to the navigation center. The attitude estimates are typically within 0.04 deg (3σ) during coasting flight, and converge to lower

values during very observable periods such as the second stage burn (around 7,000 sec) and entry (after 15,000 sec). The vehicle's rolling motion after SECO2 and the transition to CMsep attitude around 12,000 sec are clearly visible in this plot, as is the encounter with the atmosphere that makes the attitude much more observable.

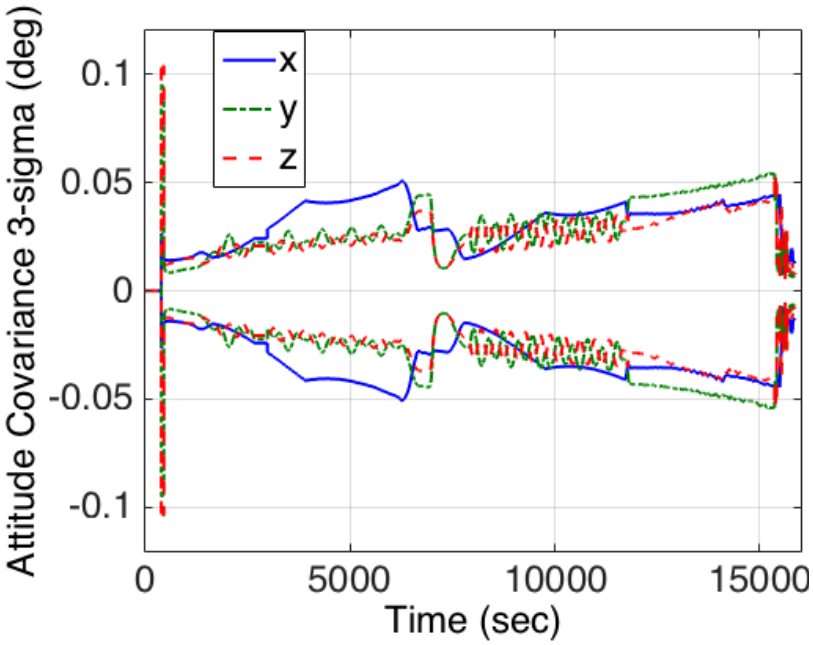

Fig. 9 CH1 Orion Body Attitude Covariance 3σ

Figures 10 and 11 shows pseudorange and delta range accept/reject counters, they show no rejected measurements for the entire flight. This fact is due to the excellent performance of the GPSR and because the filter was tuned conservatively with its measurement noise. Each line represents the number of accepted measurement for each of the 32 GPS satellites. No delta range measurement was processed after parachute deployment, the reason is the filter was tuned to process delta range only after 30 successful pseudorange measurements from the same satellite were processed. During this high dynamic phase of flight, the consecutive number of processed pseudorange measurements never reached 30.

VI. Conclusions

This paper documents the design of the Orion Exploration Flight Test 1 absolute navigation system and presents its performance during the flight. One of the flight objectives was to test

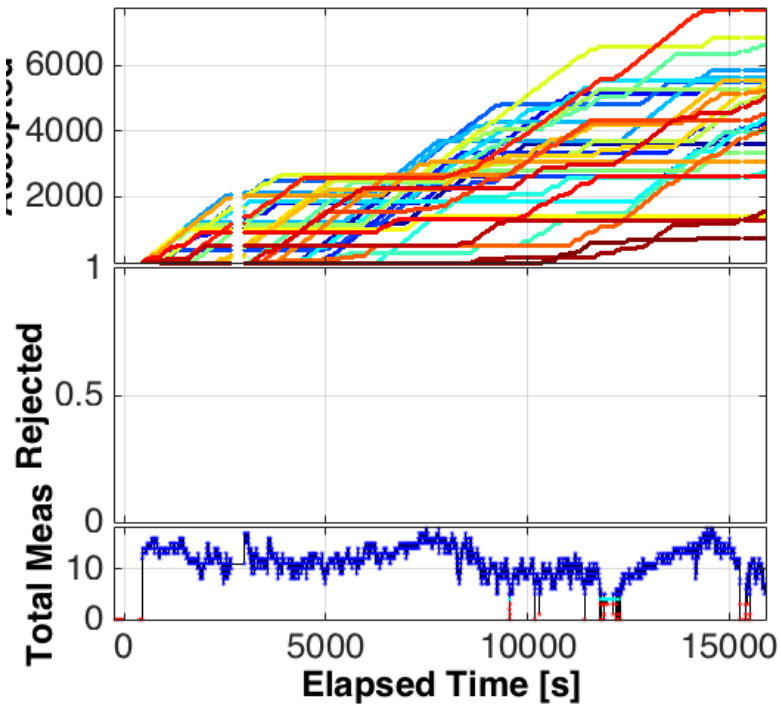

Fig. 10 CH1 Pseudorange Counters (No Rejections Occurred)

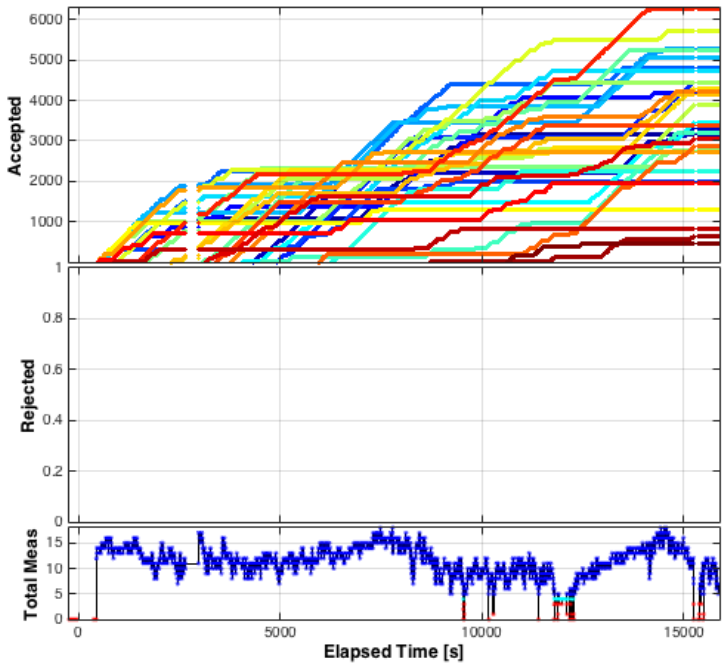

Fig. 11 CH1 DeltaRange Counters (No Rejections Occurred)

the entry system, which includes the onboard navigation using global positioning system (GPS) and inertial measurement units (IMUs). Characteristics of the design were introduced, including

the concept of navigation channel that allows for transient-less recovery from an IMU failure, a low-elevation GPS satellite masking scheme, inclusion of underweighting and consider states in the upper triangular-diagonal covariance factorization framework, and the interactions between two navigation rate groups. Data from the flight are shown to validate the design choices, and these data illustrate a flight in which the absolute navigation system performed as expected and produced a good state to guidance and control. One of the flight objectives was to test a new GPS receiver, the GPS measurement were therefore purposefully de-weighted in the filtered solution. No issues were detected in the GPS receiver performance, which in fact tracked more than three satellites all the way through apogee, beyond what was expected. No measurement rejections occurred in the filter due to a combination of good receiver performance and conservative tuning of this measurement.

References

[1] Gelb, A., editor, *Applied Optimal Estimation*, The MIT press, Cambridge, MA, 1974. pp. 182–202.

[2] Sud, J., Gay, R., Holt, G., and Zanetti, R., "Orion Exploration Flight Test 1 (EFT1) Absolute Navigation Design," *Proceedings of the AAS Guidance and Control Conference*, Vol. 151 of *Advances in the Astronautical Sciences*, Breckenridge, CO, January 31–February 5, 2014 2014, pp. 499–509, AAS 14-092.

[3] Holt, G., Zanetti, R., and D'Souza, C., "Tuning and Robustness Analysis for the Orion Absolute Navigation System," Presented at the 2013 Guidance, Navigation, and Control Conference, Boston, Massachusetts, August 19–22 2013, AIAA-2013-4876, doi: 10.2514/6.2013-4876.

[4] Bierman, G. J., *Factorization Methods for Discrete Sequential Estimation*, Vol. 128 of *Mathematics in Sciences and Engineering*, Academic Press, 1978. Chapter 5.

[5] Carlson, N. A., "Fast Triangular Factorization of the Square Root Filter," *AIAA Journal*, Vol. 11, No. 9, September 1973, pp. 1259–1265, doi: 10.2514/3.6907.

[6] Agee, W. and Turner, R., "Triangular Decomposition of a Positive Definite Matrix Plus a Symmetric Dyad with Application to Kalman Filtering," Tech. Rep. 38, White Sands Missile Range, White Sands, NM, 1972.

[7] Schmidt, S. F., "Application of State-Space Methods to Navigation Problems," *Advances in Control Systems*, Vol. 3, 1966, pp. 293–340. doi: 10.1016/B978-1-4831-6716-9.50011-4

[8] Zanetti, R. and D'Souza, C., "Recursive Implementations of the Consider Filter," *Journal of the Astronautical Sciences*, Vol. 60, No. 3–4, July–December 2013, pp. 672–685, doi: 10.1007/s40295-015-0068-7.

[9] Zanetti, R. and D'Souza, C., "Dual Accelerometer Usage Strategy for Onboard Spacecraft Navigation," *Journal of Guidance, Control, and Dynamics*, Vol. 35, No. 6, November–December 2012, pp. 1899–1901, doi: 10.2514/1.58154.

[10] Tapley, B. D., Schutz, B. E., and Born, G. H., *Statistical Orbit Determination*, Elsevier Academic Press, 2004. Chapter 4.

[11] Zanetti, R., DeMars, K. J., and Bishop, R. H., "Underweighting Nonlinear Measurements," *Journal of Guidance, Control, and Dynamics*, Vol. 33, No. 5, September–October 2010, pp. 1670–1675, doi: 10.2514/1.50596.

[12] Holt, G. and Brown, A., "Orion EFT-1 Best Estimated Trajectory Development," *AAS Guidance and Control Conference*, Breckenridge, CO, 2016, AAS 16-117.

[13] Gay, R. S., Holt, G. N., and Zanetti, R., "Orion Exploration Flight Test 1 Post-Flight Navigation Performance Assessment Relative to the Best Estimated Trajectory," Presented at the 39th AAS Guidance, Navigation, and Control Conference, Breckenridge, CO Feb 5–10 2016, AAS 16-143.

[14] Barker, L., Mamich, H., and McGregor, J., "Post-Flight Analysis of GPSR Performance During Orion Exploration Flight Test 1," *Guidance and Control Conference*, AAS, Breckenridge, CO, February 2016, AAS 16-177.

[15] Lefferts, E. J., Markley, F. L., and Shuster, M. D., "Kalman Filtering for Spacecraft Attitude Estimation," *AIAA Journal of Guidance, Control, and Dynamics*, Vol. 5, No. 5, 1982, pp. 417–429, doi:10.2514/6.1982-70.

[16] Huxel, P. J. and Bishop, R. H., "Fusing Inertial and Relative Measurements for Inertial Navigation in the Presence of Large State Error Covarianaces," *Proceedings of the 16th AAS/AIAA Spaceflight Mechanics Meeting*, January 2006.